J Mater Sci (2008) 43:4862–4869
DOI 10.1007/s10853-008-2707-x

A low-cost method for producing high-performance nanocomposite thin-films made from silica and CNTs on cellulose substrates

Emanuela Callone · Julia M. Fletcher · Giovanni Carturan · Rishi Raj

Received: 11 January 2008 / Accepted: 6 May 2008 / Published online: 3 June 2008

Abstract We show that thin films of silica loaded with 22 wt% of carbon nanotubes (CNTs) can be deposited on cellulose substrate via the sol–gel route by a well-controlled process. The high loadings are obtained by airbrush spraying of a *diluted* sol solution (which contained a much smaller concentration of CNTs) followed by drying at 200 °C. The films are nearly continuous despite the fibrous structure of the substrate. The high degree of connectivity of the stranded structure of the CNTs yields a specific electrical conductivity of $3 \times 10^3\ \Omega^{-1}\ m^{-1}$. In contrast, films made with high loadings of carbon black have poor electrical conductivity. Results from mechanical tensile tests of samples are also reported. This economical method of producing CNT dispersed thin films could find application in catalysis, as electrodes in fuel cells and batteries, and in sensor technologies.

Introduction

Carbon nanotubes (CNTs) are high-surface area materials that can be functionalized by molecular layering [1]. These functionalities combined with the high electronic conductivity of CNTs [2] make then promising candidates for electrodes, catalysis, and sensor applications [3–6]. These applications require fabrication of CNTs into forms that can be handled with ease. One process consists of dispersing CNTs like an ink followed by filter-pressing into a matted structure, yielding a paper-like structure. Typically, the paper produced by such a process is approximately 100 μm thick, with an interconnected porosity on the scale of about 25 nm. In many applications, the fine porosity restricts the access of surface-active species, as for example in catalysis, to the interior of the paper. Thus thin film CNT structures are likely to provide higher efficiencies when the performance is normalized with respect to per unit weight of the CNTs. Also, technological applications require a low-cost processing method for production and implementation of CNT-based thin films.

In this article, we report an alternative method for fabrication of CNT-based thin films. The homogeneous films are obtained through deposition, by spraying, of a dilute solution of silica sol containing CNTs, onto a substrate made from ordinary cellulose fibers. The sol-dispersion is sprayed using an airbrush, followed by air drying which increases the concentration of the CNTs in the thin films to high levels. This low-cost process can easily adapt to different types of scaffolds, such as textiles. Thus, the process is amenable to large-scale manufacturing [7, 8].

In the present work, the CNT films are deposited on substrates made from cellulose. Such substrates are being considered for electronic display screens, nanotubular ITO sheets, nanofibers for air filtration, and as supports for composites made from hydroxyapatite, TiO_2, and titanium apatite [9–11]. In the present application the cellulose has the advantage that it is chemically compatible with the silica sol [12, 13]. While other porous materials may require chemical treatments to create molecular anchors that bond to the coating, the cellulose provides its own −OH groups that can react with the residual Si–OH or

E. Callone (✉) · G. Carturan
Department of Materials Engineering and Industrial Technologies, University of Trento, via Mesiano 77, 38050 Trento, Italy
e-mail: emanuela.callone@ing.unitn.it

J. M. Fletcher · R. Raj
Department of Mechanical Engineering, University of Colorado, Boulder, CO 80309-0427, USA

Si–OR groups of the hydrolyzed silica sol. The cellulose substrate is ashless; it does not leave a residue when oxidized in air. Therefore, self-standing thin films can be made simply by "burning" the substrate in air.

The airbrush spraying method, eventually, provides a uniform coating over the fibrous structure of the cellulose substrate [14], which is not possible by dip or spin coating. An airbrush is a tool that sprays various media (ink, dye, paint) through the atomization process: a stream of compressed air is forced through a venturi aspirator, causing a local reduction in air pressure that allows "ink" to be pulled up from a reservoir, at normal atmospheric pressure, connected to the nozzle. The high speed of the air and the trigger, which opens a fine tapered needle controlling the amount of paint, produce an extremely fine droplet (atomization) ensuring an excellent dispersion of the solution. There are different types of airbrushes classified by three characteristics: (i) the trigger action to control the paint flow, (ii) the mechanism of paint feeding into the airbrush, and (iii) the mixing point of paint and air.

The technique is based on the freehand manipulation of the airbrush, medium, air pressure, and distance from the surface being sprayed in order to produce a definite reproducible and predictable result. To increase the reproducibility of the coating layer it is possible to automate the process by building a clean chamber equipped with a mechanical arm able to move on an x–y plane in front of the surface to be coated; the airbrush is mounted on it. Thus, the intensity, speed, and the position of the flow can be remote controlled. The techniques are commonly used in very different fields of everyday life such as illustration, photo-retouching, coating firearms, murals, temporary airbrush tattoos, airbrush tanning, finger nail art, clothing, automotive [14].

In the scientific research field, the inkjet printing, which is an example of airbrush spraying, is used to deposit Ag and Cu inks, to make thin films made of a silica gel [15, 16], and to deposit nanoparticles with functional properties [17–19]. Similarly, carbon black (CB) [20, 21] as well as CNT [22] are used to form thin films or composites with specific tailored properties.

In this work, two types of composites, one made from CB and the other with carbon-nanotubes, were chosen in order to compare the influence of the size and the shape of the carbon phase on the properties of the composite. A carbon-free silica-sol sample was prepared as a control. These three kinds of samples are called: (i) *100Si*, silica-sol coating without carbon loading, (ii) *150 SiCB*, sols dispersed with CB, and (iii) *44SiCNT*, sols dispersed with CNTs. The airbrush process produced films with thicknesses in the 7–50 μm range. The thickness was controlled by depositing the film in several cycles (up to 10). The carbon fraction in the composites was kept constant; these loadings are near the upper limit that can be produced by the present process.

Experimental methods

Materials

Blue ribbon ashless filter paper, weighing 85.7 g/m^2, and with a thickness of 130 ± 30 μm, was purchased from Schleicher & Schüll. HiPco nanotubes (Carbon Nanotechnologies Inc., Houston, Tx) and Carbon Black (EC300J, Akzo Nobel Chemicals SA, Barcelona, Spain) were crushed in a mortar, sieved below 32 μm, heated under N_2 at 110 °C for 2 h, and stored in dry conditions in the presence of P_2O_5. *Tetra*ethoxysilane (TEOS, purity 99%), solvents, and other chemicals were supplied by Sigma–Aldrich and used without further purification.

Sample preparation

A disk, 10 cm in diameter, was cut from the paper and secured to a glass plate by paper clips: thus made ready for airbrush spraying. The coating was applied in 10 cycles; the sample was dried in an air-oven at 80 °C for 30 min after each cycle. Each coating cycle required 1 min to ensure uniform coverage of the sample. This procedure was determined from preliminary experiments with diluted blue ink and visual inspection for homogeneity of the deposition. The airbrush nozzle had a diameter of <500 μm; it was immediately cleaned after each use with acetone and deionized water to avoid clogging. Several paper disks were treated in this way and then cut in strips of about 20 × 2.5 mm (L × W). Fully coated samples were heated under N_2 at a rate of 100 °C/h to the final temperature of 200 °C and held at this temperature for 2 h. These samples were now ready for physical characterization.

The 100Si sample was prepared by mixing 18.6 mL of TEOS with 27 mL of EtOH and 4.5 mL of 1×10^{-2} M HCl solution (nominal SiO_2 concentration = 100 g/L; TEOS/H_2O molar ratio = 1/4). The solution was stirred for 6 h before use and stored at 4 °C. The suspension for 150SiCB was prepared by mixing 0.25 g of CB powder with 5 mL of 100Si sol with vigorous mixing for 30 min. The CNT sample, 44SiCNT, was prepared by adding 0.02 g of CNTs to 2 mL of 100Si sol diluted with 3 mL of deionized water. The suspension was put in an ultrasonic bath for approximately 2 h. The homogeneous suspension was kept stirred up to just before spraying.

The total mass of the coating was measured by weighing the samples before and after the coating. The mass was normalized with the surface area of the paper scaffold and is given in units of mg m^{-2} in Table 1. Portions of the

Table 1 Physical features of coated and uncoated samples, as well as the carbon constituent

Sample	Mass deposit[a], g/m^2 (±10%)	Exp. SSA, m^2 g^{-1} (±5%)	Calc. SSA[b], m^2 g^{-1}	Mean pore diam., Å (±10%)	Effective film thickness, μm	Normalized thickness[c]
Paper	n/a	3	n/a	384	n/a	n/a
100Si	57	18	20	26	8.0	14.0
150SiCB	86	163	161	20	44.5	51.7
44SiCNT	19	20	18	65	7.4	39.0
CB	n/a	853	n/a	51	n/a	n/a
CNT	n/a	489	n/a	90	n/a	n/a

[a] Paper weight: 85.7 g/m^2

[b] Calculated SSA of SiO_2: 45 m^2/g

[c] Per 100 g/m^2 of deposit

three types of suspensions were stored separately to complete the condensation process. These gels, named 100Si*, 150SiCB*, and 44SiCNT*, were ground into powders for TG-MS and FTIR analyses.

The airbrush spray coating produced predictable results: the actual weight of the films deviated by less than 10% from the value expected from the carbon loadings in the sol. For example, the 57 g m^{-2} mass deposited in 100Si is equivalent to an effective sprayed volume of 570 mL (in 10 spray cycles) of the sol, which contained 100 g/L of solids. In the case of 150SiCB, the 86 g m^{-2} specific mass deposit corresponds to 570 mL of sol containing 150 g/L of solids (SiO_2 + CB). The 44SiCNT sample shows a 19 g/m^2 of mass addition, determined by spraying 430 mL of the sol containing 44 g/L of solids (SiO_2 + CNT).

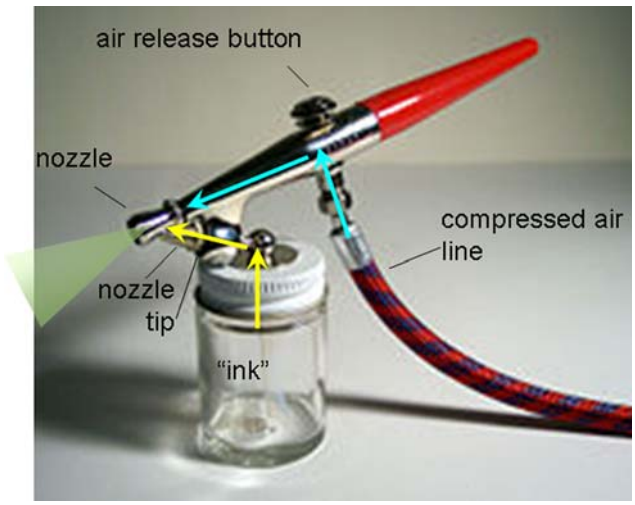

Scheme 1 Paasche F#1 single action external mix airbrush

Instruments and measurements

The coatings were prepared with a hand-held single action external mix airbrush (model F#1, Paasche Airbrush Company, Chicago, IL), powered by compressed air at 4 bar, with the nozzle exit being held at a distance of 10 cm from the substrate mounted on a hot plate for a uniform and fast evaporation of the solvent. With this equipment only one action is required for operation. The depression of the trigger releases a fixed ratio of sol to air. The selection of tip and nozzle combination and adjusting manually the spray volume achieve specific line width (Scheme 1).

Microstructural analysis was carried out on a JEOL JSM 5500 scanning electron microscope (SEM) at 100, 50, and 10× magnification at 10 kV (20 kV for EDX).

FTIR spectra were recorded on a Nicolet Avatar 330 spectrometer in transmission mode in the 4000–400 cm^{-1} range. Powdered samples were analyzed in KBr pellets by collecting 64 scans with 4 cm^{-1} resolution.

Specific surface areas and pore size values were determined by N_2 adsorption at 77 K with an ASAP2010 Micromeritics analyzer. Equilibrium points were considered inside the 0.05–0.33 p/p_0 range; data were processed by BET and BJH equations. All samples produced Type II adsorption isotherms (IUPAC classification).

Thermogravimetric (TG) analysis was performed on a LabSys Setaram thermobalance operating in the 20–1000 °C range, with a heating rate of 10 °C min^{-1}, under 100 cm^3 min^{-1} He flow. Samples were analyzed by using a 0.4 cm^3 alumina crucible. The thermobalance is connected to a VG-QMD-1000 Carlo Erba Instruments quadrupole mass spectrometer by a thermostatted transfer-line. Electron impact mass spectra (70 eV) were continuously registered and stored with frequency of 1 scan s^{-1} ranging from 2 to 500 amu. The TG-MS instrumental interface, experimental procedure, and data processing adopted in this study are described elsewhere [23].

Electrical conductivity measurements were made on 20×(2–3) mm ribbons, with a thickness of 0.16 ± 0.03 mm. Silver paste at the ends served as the electrodes. The resistance was measured from the slope of the current versus voltage data. Linear Ohmic behavior was confirmed for all measurements. The specific conductivity, σ, was calculated from the resistance and the sample geometry. The measurements have a total uncertainty of ±5%. The active cross section of the deposited film was calculated as the difference between the sample and the uncoated paper thicknesses, measured three times on various points of the strips.

Mechanical measurements were carried out in uniaxial tension in an Instron Corporation model 4502-Series IX universal testing machine, equipped with a 10 N load cell. The samples are $20\times(2–3) \times 0.16 \pm 0.03$ mm of size ($L \pm W \pm T$). The tests were carried out at 23 °C and 50% relative humidity, at a crosshead speed of 1 mm/min. The displacement in the gage length was measured with a displacement transducer. Ten specimens for each composition were tested.

Results and discussion

Structure and morphology

SEM micrograph of the bare cellulose substrate is given in Fig. 1a, and after coating with silica (100Si) in Fig. 1b. The silica deposit is homogeneous. Individual cellulose fibers can be seen to be entirely coated with silica (Fig. 1b); this was further confirmed from energy dispersive X-ray (EDS) maps of the surface.

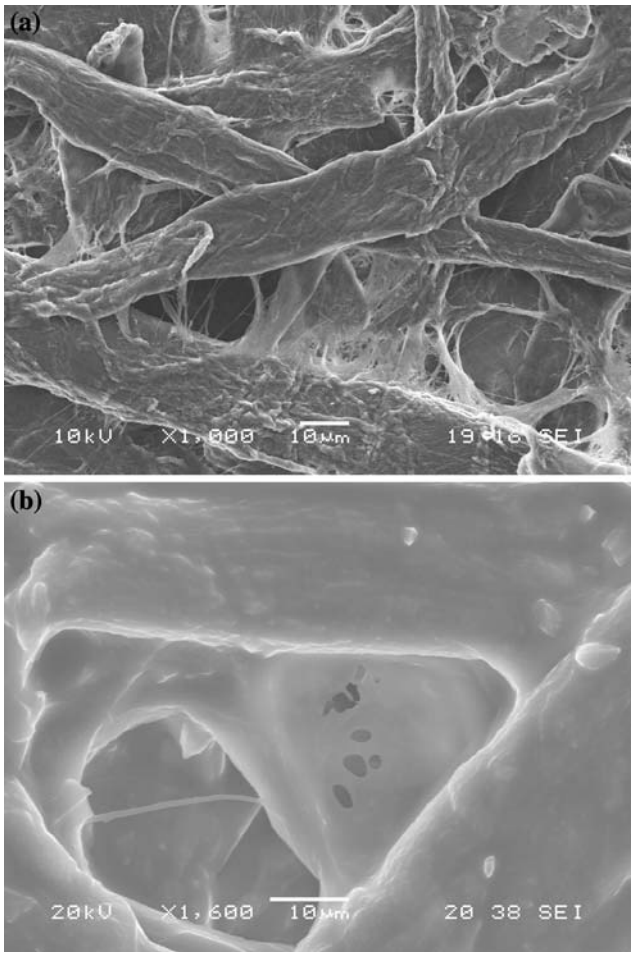

Fig. 1 SEM images of paper samples: (**a**) original filter fibers and (**b**) after coating with 100Si sol

The addition of CB and CNTs to the silica sol changes the morphology of the coating. SEM micrographs of the 150CB sample are given in Fig. 2a. The surface of this sample appears globular because inter-fiber spacing of the substrate has been filled with "droplets" of the carbon black. In contrast, the coating in the 44SiCNT sample, shown in Fig. 2b, forms a nearly continuous thin film that forms "blanket" over the substrate, apparently because the long strands of the CNTs serve to bridge over the fibers in the substrate. At the chosen magnification it is not possible to distinguish the "filler" (CB or CNT) of the silica matrix. The pictures are interesting for a surface's appearance comparison with the images in Fig. 1. Figure 2a shows a surface with a lot of cracks and the morphology of the cellulose fibres is lost; this is maintained when coated with pure silica sol (Fig. 1b) and it is still visible in the sample coated with CNT-silica sol (Fig. 2b). This suggests that the CB particles are not really ideal and inert filler, because the coating layer masks completely the support.

Figure 3 gives evidence of a uniform distribution of the CNTs within the film. Note that the CNTs are embedded within the film, rather than segregating to the surface of the film. The homogeneity of the CNT nanocomposite thin film is attributed to a rapid condensation of the sol on the substrate. This result was achieved by optimizing the $Si/H_2O = 4$ ratio, and the 2 h of ageing time, based upon the study of the TEOS gelling process [24–26], and to the drying due from the hot plate used as support. Furthermore, the point at which carbon solids were added to the sol had to be optimized so that the sol was fluid enough to avoid clogging of the airbrush nozzle, but sufficiently aged to condense quickly on the cellulose fibers. In this way agglomeration of the carbon phase could be avoided.

The physical characteristics of the films, paper, as well as of the CB and of the CNTs are summarized in Table 1.

In the N_2-physisorption analysis, all samples produced Type II adsorption isotherms (IUPAC classification). The pore size distributions (PDS) are dominated by the mesoporosity of the paper texture, in rough agreement with the presence of different materials (i.e., paper, silica xerogel, and carbons), which present large adsorption due to the micropores [27]. For example, the data for 44SiCNT give the mass deposit on the substrate to be 19 g m^{-2}, and the SSA of the coating and the substrate taken together as 20 m^2 g^{-1}. The mean pore diameter in this sample is 6.5 nm, while the pore diameter for just the substrate is 38.4 nm. The specific surface area values for the composites agreed reasonably well with the rule of mixture predictions obtained from the silica and carbon constituents. The inference is that the CB and the carbon-nanotubes do not react with the silica gel, and thus retain their original structure.

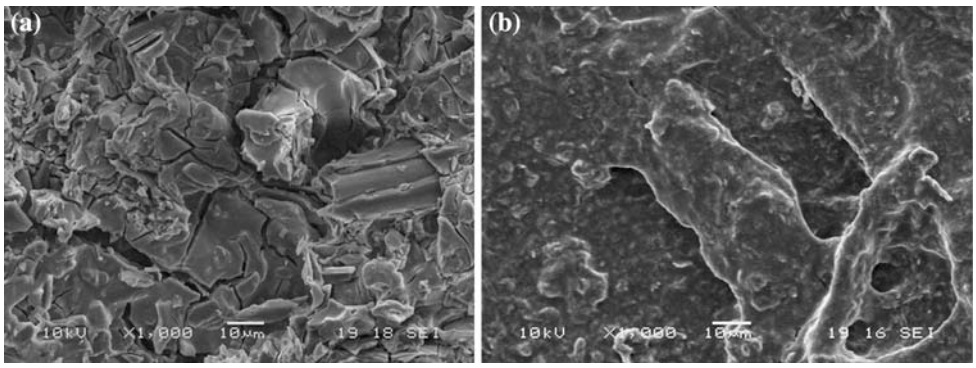

Fig. 2 SEM micrographs of (**a**) 150SiCB and (**b**) 44SiCNT

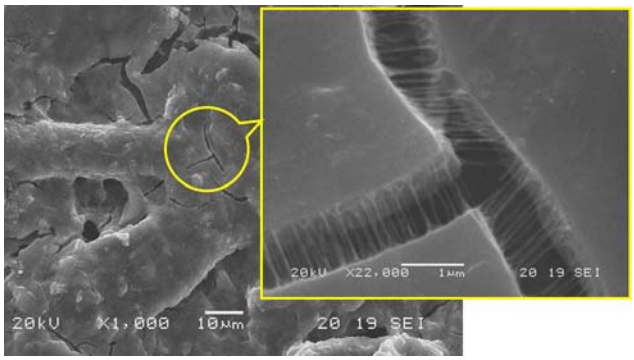

Fig. 3 The CNTs are shown to be embedded within the silicon film, as well as bridging microcracks in the film

The film thickness was measured by comparing the total thickness of the coated substrate and the untreated paper. The thickness of the untreated paper was 135.6 μm. The values given in Table 1 represent the average of 10 measurements. The right-hand column gives the effective thickness of the film normalized for 100 g/m^2 of deposit. The lower number for 100Si, relative to the carbon containing samples, reflects the seeping of the sol into the paper, which appears to be prevented by the presence of carbon particles in the sol.

TG analysis coupled with MS identification of pyrolysis gaseous products was carried out under inert gas flow. The results from the paper samples 150SiCB and 44SiCNT are given on the left in Fig. 4. The total mass loss in these specimens is 81.9%, in the 200–500 °C interval, which is due mainly to H_2O and CO_2.

To consider only the behavior of the coating material the analyses were run also on the original gels, in the form of dried powder aged in the same way of the films. Results from 150SiCB* and 44SiCNT* are shown on the right in Fig. 4. In these samples the total mass loss is quite low (<5%), which arises from the release of ethanol (m/z 31,

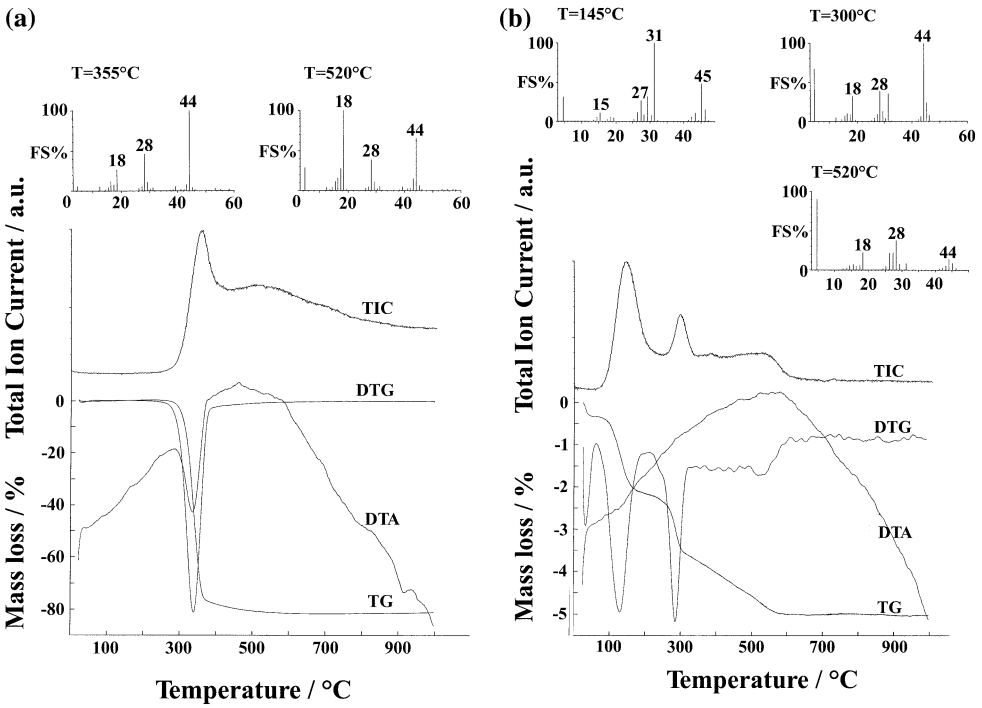

Fig. 4 TG-MS data of the paper scaffold (left) and of the 150SiCB gel without paper (right)

46) at 130 °C, and H_2O (m/z 18), ethylene (m/z 28) and ethanol above 250 °C. We conclude that the thermal behavior of carbon-coated samples, 150SiCB and 44SiCNT, is dominated by the pyrolysis of the (ashless) paper. For example, 150SiCB shows a total mass loss of 42.4%. Considering the 171.8 g/m^2 weight, i.e., the sum of paper (85.7 g/m^2), SiO_2 (57.4 g/m^2), and CB (28.7 g/m^2), the experimental 42.4% loss corresponds to 69.9 g/m^2 which agrees with the value of 70.1 g/m^2 calculated from the 81.9% weight fraction of the cellulose.

The condensation between residual Si–OH and Si–OEt and the elimination of Si–OEt account for these mass-spectrometric data [28]. It is noteworthy that, after drying at 80 °C, the silica xerogel is already constituted by an almost complete Si–O network, according to the very low mass loss caused by the condensation of the residual terminal Si–OH and Si–OEt groups.

FTIR spectra for the gelled samples, 100Si*, 150CB*, and 44CNT*, heat-treated at different temperatures are given in Fig. 5. All samples show signals from Si–O–Si at 1075, 790, and 447 cm^{-1}. The Si–OH peak at 941 cm^{-1} confirms the siloxane network formation. The small peaks centered at around 1630 and 2925 cm^{-1}, present in all samples, refer to −OH and C–H species. These species are present in the low-temperature 100Si* specimens. In other samples they show the chemisorption of water and other organics on activated carbon at 900 °C [29, 30].

Both spectrometric and spectroscopic data indicate the presence of functional groups present on the samples that are responsible for the variation of performances with temperature. The xerogels show a minor presence of adsorbed water and uncondensed Si–OR groups that may interact with −OH of the cellulose to anchor the film to the substrate. Then, heating leads to higher condensation, which affects mechanical and electrical properties, as described below. Condensation increases the mechanical stiffness.

The stability of the IR patterns in the carbon containing specimens, even upon annealing to high temperatures, suggests that the carbon constituents behave as inert filler in the silica matrix.

Electrical behavior

The specific conductivity of the samples is reported in Table 2. The low value of the 100Si is expected, since silica and cellulose are insulators [31, 32]. However, the conductivity goes up to 3×10^{-3} Ω^{-1} m^{-1} for 150SiCB sample, and then dramatically to 3×10^{4} Ω^{-1} m^{-1} for 44SiCNT. The behavior of the coatings, consisting of silica-carbon composites, is obtained by assuming that the experimental values of the conductivity arise predominantly from the coating (which is measured by subtracting the thicknesses of the coated and uncoated samples). These data correlate with the morphology of carbon. In 150SiCB, the approximately spherical shape of the carbon particles,

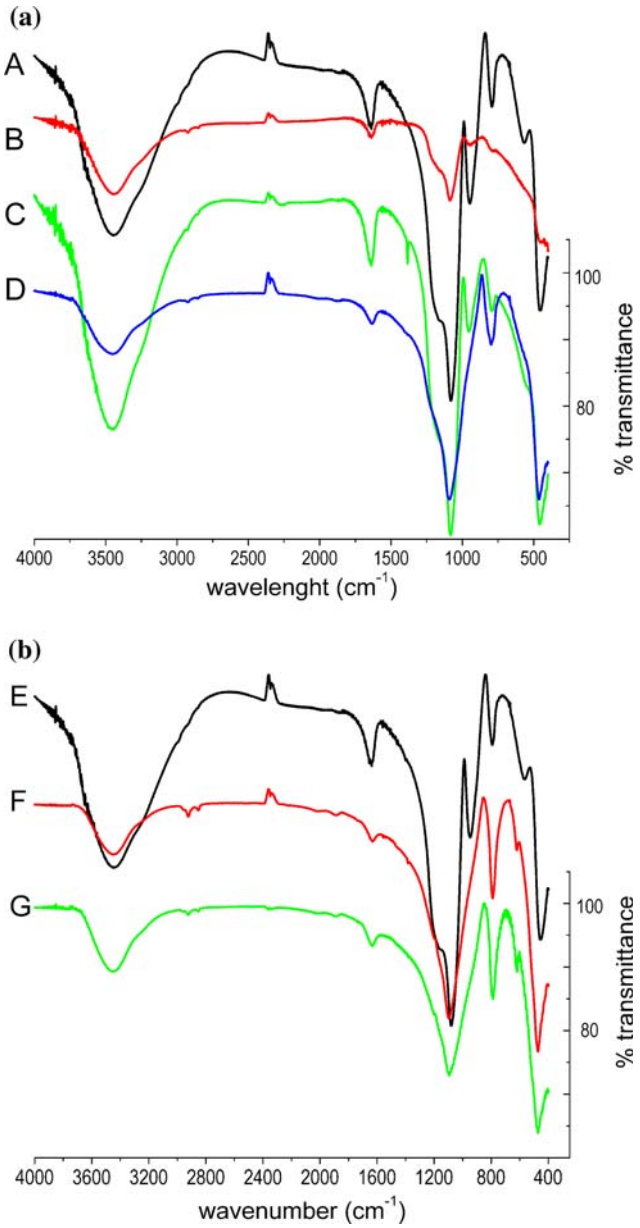

Fig. 5 FTIR spectra of doped SiO_2 gels treated at various temperatures: (A) TEOS gel at RT; (B) 44SiCNT at RT; (C) 44SiCNT at 200 °C; (D) 44SiCNT at 900 °C; (E) 150SiCB at 25 °C; (F) 150SiCB at 200 °C; and (G) 150SiCB at 900 °C

Table 2 Comparison among conductivity values of the whole samples and the coating materials alone

Sample	σ of the composite (Ω^{-1} m^{-1})	σ_{EFF} of the coating (Ω^{-1} m^{-1})
100SiO_2	<0.0005	n/a
150SiCB	0.003	0.01
44SiCNT	12.5	3000

and the cracks present in the coatings, apparently impede the development of well-connected CB particle-structures. On the other hand, the fibrous structure of the carbon nanotubes in 44SiCNT favors only to a minor extent (in comparison with CB particles) the development of shrinkage cracks in the films, but also contributes to the creation of an interconnected network.

The nominal shrinkage in sol–gel siliceous products [33] results in thickness decrease with progressive stiffening. In the composites, the CNTs remain dispersed in the liquid phase, and gradually gather to higher concentrations with overall shrinkage. Thus, the silica gel shrinkage leads to a uniform distribution of CNTs in the silica layer producing a "frozen nano-net". The tubular shape of the CNTs perhaps also counters their tendency to aggregate. The presence of CNT also bridges the cracks that may develop in the silica overlayer during condensation, as seen in Fig. 3.

The intrinsic conductivity of CB is lower than that of CNTs [34, 35], which may explain why the 150SiCB coating is less conducting than the 44SiCNT coating. The specific conductivity of 44SiCNT is more or less consistent with the intrinsic values proposed for naked CNTs ($\sim 10^5\ \Omega^{-1}\ m^{-1}$) and the volume fraction of the nanotubes in the silica-matrix [36].

Mechanical testing

Samples were aged at room temperature for 2 months before mechanical testing. The stress–strain curves are given in Fig. 6. The results for the Young's modulus, E, the fracture strength, σ_F, and the strain at fracture, ε_F, are reported in Table 3.

The most striking result in Fig. 6 is the high elastic modulus and the fracture strength of 100Si. In this sample, the fibers in the cellulose paper were uniformly coated with

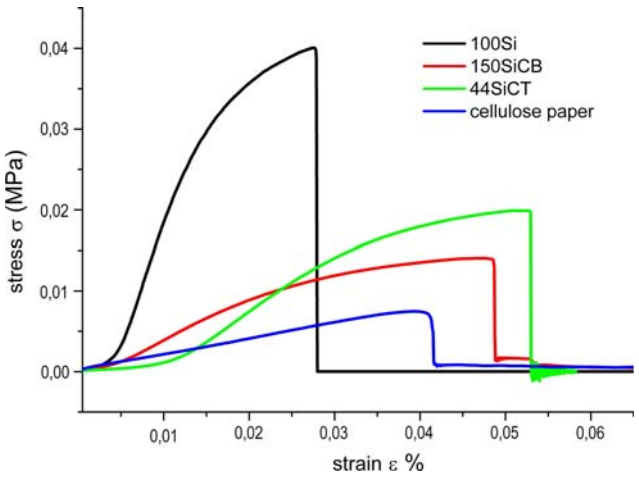

Fig. 6 Averaged tensile stress curves of the samples stabilized and aged

Table 3 Tensile strength data of samples, taken as averages of several measurements at different strips

Sample	E (MPa)	σ_F (MPa)	ε_F (%)
Paper	430 ± 55	11 ± 1	3.5 ± 0.5
100Si	2894 ± 409	36 ± 4	2.1 ± 0.2
150SiCB	520 ± 46	11 ± 1	3.5 ± 0.7
44SiCNT	957 ± 148	19 ± 5	3.0 ± 1.1

sol–gel derived silica. This silica coating of the fiber significantly stiffens the cellulose substrate. The −OH group in cellulose fibers react with the Si–OH groups in the sol, creating strong bridging bonds between the coating and the fibers; this may have produced a "welding" of the fibers to one another, inhibiting slippage among the fibers and thereby enhancing the effective elastic modulus. This bonding mechanism has been proposed by Carturan et al. [37] for thin sol–gel coatings on silk fibers that were deposited by means of a vapor phase of silicon alkoxide [38, 39].

While the silica gel formed coatings on individual fibers in the cellulose substrate, as discussed above, the coatings in 150SiCB and 44SiCNT formed a separate surface layer on the cellulose substrate. Therefore, the effect of the coatings on the overall elastic modulus of the samples was weaker. The higher stiffness of the carbon-nanotubes sample as compared to the CB sample most likely reflects the higher integrity of the film: in 150SiCB the coating appeared to have many cracks, while coatings in 44SiCNT had a higher degree of continuity.

Conclusions

The production of efficient nanocomposites is evaluated taking into account some physical properties resulting from the sum of components, focusing on geometry, morphology, and the reproducibility of the preparation procedure.

In conclusion, this work demonstrates that silica sol suspensions loaded by CNT or CB can effectively be sprayed on low-cost scaffolds, such as paper, resulting in a homogeneous and continuous silica deposit on the paper fibers. The process provides reliable and reproducible results. In particular, the possibility to obtain high electrical conductivity as in the case of SiO_2 + CNT specimens is especially promising. The observed improvement of E and σ_F values of paper after SiO_2-sol soaking is consistent with the formation of Si–O-cellulose bonding. The proposed results put the proposed material in the category of nanocomposites characterized by the presence of fillers of various shapes and sources to produce a reinforcement of the matrix.

Acknowledgements The authors thank Prof. Ing. A. Pegoretti and Dr. Matteo Traina for mechanical tests and useful discussions. Julie Fletcher received support by a grant from the National Science Foundation from the Ceramics Program of the Division of Materials Research: DMR-0502446.

References

1. Felten A, Bittencourt C, Pireaux JJ (2006) Nanotechnology 17:1954. doi:10.1088/0957-4484/17/8/026
2. Thorat IV, Mathur V, Harb JN, Wheeler DR (2006) J Power Sources 162:673. doi:10.1016/j.jpowsour.2006.06.032
3. Campbell IM (1988) Catalysis at surfaces. Kluwer Academic Publishers, London
4. Rioux RM, Song H, Hoefelmeyer JD, Yang P, Somorjai GA (2005) J Phys Chem B 109(6):2192
5. Jung LS, Campbell CT, Chinowsky TM, Mar MN, Yee SS (1998) Langmuir 14(19):5636
6. Nigge U, Wiemhöfer H-D, Römer EWJ, Bouwmeester HJM, Schulte TR (2002) Solid State Ionics 146(1–2):163
7. Keszei S, Matko S, Bertalan G, Anna P, Marosi G, Toth A (2005) Eur Polym J 41:697 doi:10.1016/j.eurpolymj.2004.10.039
8. Cai LF, Mai YL, Rong MZ, Ruan WH, Zhang MQ (2007) eXPRESS Polym Lett 1(1):2
9. Andersson P, Nilsson D, Svensson P-O, Chen M, Malmström A, Remonen T, Kugler T, Berggren M (2002) Adv Mater 14(20):16
10. Aoki Y, Huang J, Kunitake T (2006) J Mater Chem 16:292. doi:10.1039/b512225b
11. Grafe T, Graham K (2003) Int Nonwov J 12:51
12. Trepte J, Bottcher H (2000) J Sol-Gel Sci Technol 19:691. doi:10.1023/A:1008766807514
13. Mahltig B, Ffiedler D, Bottcher H (2004) J Sol-Gel Sci Technol 32:219. doi:10.1007/s10971-004-5791-7
14. (a) Chou TP, Cao G (2003) J Sol-Gel Sci Technol 27:31. doi:10.1023/A:1022675809404; (b) Downie R (2001) How to use an airbrush. Kalmbach Publishing Co., Waukesha, WI
15. Curtis CJ, Schulz DL, Miedaner A, Alleman J, Rivkin T, Perkins JD, Ginley DS (2001) Mater Res Soc Symp Proc 676:861
16. (a) Watson KA, Smith JG Jr, Connell JW (2003) Space durable polyimide/carbon nanotube composite films for electrostatic charge mitigation. NASA Langley Technical Library Digital Repository, New York; (b) Baker GL, Ghosh RN, Osborn DJ III, Zhang P (2005) Fibre optical micro-detectors for oxygen sensing in power plants. DOE Quarterly Technical Report, New York
17. Gojny FH, Wichmann MHG, Fiedler B, Schulte K (2005) Comp Sci Technol 65:2300. doi:10.1016/j.compscitech.2005.04.021
18. Vasenka J, Manne S, Giberson R, Marsh T, Henderson E (1993) Biophys J 65:992
19. Schmid G (ed) (2004) Nanoparticles: from theory to application. Wiley-VCH Verlag, Weinheim
20. Deng Y, Deng C, Yang D, Wang C, Fu S, Zhang X (2005) Chem Commun 5548
21. Takasu Y, Kawaguchi T, Sugimoto W, Murakami Y (2003) Electrochim Acta 48:3861. doi:10.1016/S0013-4686(03)00521-8
22. Péna-Alonso R, Sicurelli A, Callone E, Carturan G, Raj R (2007) J Power Sources 165:315. doi:10.1016/j.jpowsour.2006.12.043
23. Campostrini R, Ischia M, Palmisano L (2003) J Therm Anal Calorim 71:997. doi:10.1023/A:1023307100279
24. Sivananda SJ (1987) J Am Ceram Soc 70(11):C-298
25. Sanchez J, McCormick A (1992) J Phys Chem 96:8973. doi:10.1021/j100201a051
26. Brinker CJ, Keefer KD, Schaefer DW, Ashley CS (1982) J Non-Cryst Solids 48:47. doi:10.1016/0022-3093(82)90245-9
27. Li F, Wang Y, Wang D, Wei F (2004) Carbon 42:2375. doi:10.1016/j.carbon.2004.02.025
28. Campostrini R, D'Andrea G, Carturan G, Ceccato R, Soraru' GD (1996) J Mater Chem 6:585. doi:10.1039/jm9960600585
29. Vinogradova E, Estrada M, Moreno A (2006) J Colloid Interface Sci 298:209. doi:10.1016/j.jcis.2005.11.064
30. Pan G, Mark JE, Schaefer DW (2003) J Polym Sci B Polym Phys 41:3314. doi:10.1002/polb.10695
31. Warren WL, Lenahan PM, Brinker CJ, Shaffer RG, Ashley CS, Reed ST (1990) Mater Res Soc Symp Proc 413
32. Hübert T, Shimamura A, Klyszcz A (2005) Mater Sci – Poland 23:1
33. Chen Y, Zhang Z, Sui X, Brennan JD, Brook MA (2005) J Mater Chem 15:3132. doi:10.1039/b502959g
34. Fan Z, Wei T, Luo G, Wei F (2005) J Mater Sci 40:5075
35. Colbert DT (2003) Plastics Additives & Compounding
36. Kasumov AY, Khodos II, Ajayan PM, Colliex C (1996) Europhys Lett 34:429. doi:10.1209/epl/i1996-00474-0
37. Carturan G, Khandelwal N, Tognana L, Sglavo VM (2007) J Non-Cryst Solids 353:1540. doi:10.1016/j.jnoncrysol.2007.01.037
38. Sglavo VM, Carturan G, Dal Monte R, Muraca M (1999) J Mater Sci 34:3587. doi:10.1023/A:1004626632730
39. Christie JH, Woodhead IM (2002) Textile Res J 72:273. doi:10.1177/004051750207200315